36A.0 MICROSTRUCTURAL EVOLUTION IN TITANIUM ALLOYS UNDER ADDITIVE MANUFACTURING CONDITIONS

Student: Alec Saville (Mines)
Faculty: Amy Clarke (Mines)
Industrial Mentor(s): Adam Pilchak (AFRL), Collin Donohoue (SNL), and Jessica Buckner (SNL)

This project started in Fall 2018 and was initially supported by the Office of Naval Research. This project is currently supported by the National Science Foundation Graduate Research Fellowships Program (NSF GRFP). The research performed during this project will serve as part of the basis for a Ph.D. thesis program for Alec Saville.

36A.1 Project Overview and Industrial Relevance

Over the last decade, metallic additive manufacturing (AM) has seen increasing use in the creation of near-net shape, functional and low-risk structural components. The primary benefit of AM over traditional processing is the ability to create custom geometries beyond what is possible with traditional manufacturing and to reduce the waste associated with extensive machining [36.1-4]. One of the primary challenges to AM is maintaining control of microstructure and properties via careful selection of build parameters. Defects, including porosity and cracking, along with anisotropic loading responses and detrimental microstructural formations are all possible in AM builds, limiting metallic AM parts to low-risk applications [36.5-8]. The influence of processing parameters (e.g., scan strategy or layer thickness) on microstructure and defect development is not well-understood, and is an active area of materials research.

This project focuses on evaluating how AM of the ubiquitous titanium alloy Ti-6Al-4V responds to changes in build parameters and processing conditions, while also exploring new avenues for microstructural refinement in emerging titanium alloys designed for AM. Samples of electron beam melted (EBM) Ti-6Al-4V produced with varying scan startegies and Wire-arc AM (WAAM) Ti-6Al-4V from a large-volume build are being evaluated to elucidate how changes in build parameters within the same build process (e.g., scan strategy), or changes between build process (EBM vs WAAM) alter microstructure development. Exploration of microstructural refinement during AM builds with an emerging class of Ti-Cu alloys is also planned as part of this work.

The three specimens of EBM Ti-6Al-4V were produced at Oak Ridge National Laboratory (ORNL) with different scan strategies identified as Raster, Dehoff, and Random. Random and Dehoff are spot melt methods, depositing material in spots instead of in a linear fashion (**Figure 36.1)**. Raster is a traditional deposition process, whereby powder is melted linearly for every layer, and then the travel path is rotated 67.5° between layers (**Figure 36.2)**. The WAAM specimens were produced at Sandia National Laboratory (SNL) in a large-bowl build geometry using argon shielding gas (**Figure 36.3**).

36A.2 Previous Work

36A.2.1 EBM Ti-6Al-4V Neutron Diffraction and EBSD Texture Measurements

Neutron diffraction measurements were completed at the High-Pressure-Preferred-Orientation (HIPPO) beamline at Los Alamos National Labortaory (LANL) as a function of build height and scan strategy. Rietveld refinement of the neutron diffraction results was completed using the Material Analysis Using Diffraction (MAUD) software version 2.33 to generate information about crystallographic preferred orientations (texture). Systematic implementation of this software has resulted in the creation of an updated tutorial document currently in preparation for the journal *Integrating in Materials and Manufacturing Innovation*. Complimentary large-scale EBSD mapping (4 x 4 mm by area) was also completed as a function of build height and scan strategy to link microstructural features to specific texture components, and to enable reconstruction of the as-solidified microstructure and orientations.

Previously completed work has shown that EBM α-Ti texture does not noticeably change as a function of build height, but changes in response to scan strategy (**Figure 36.4**). Quantification of the primary α-Ti texture components illustrate clear differences, when completed using the Bunge angle convention and a triclinic specimen symmetry. This latter assumption was made given the asymmetry of the orientations observed previously (**Figure 36.4**). Previous studies implemented an orthotropic specimen symmetry, which neglects the presence of any such asymmetry in orientations across the specimen reference frame, and can render a study of crystallographic texture

incomplete [36.9-12]. For traditional manufacturing processes like rolling, this is not usually an issue, but AM build processes may not symmetrically produce orientations within a build. Thus, triclinic specimen symmetry is more appropriate. This effort also revealed a lack of a constant reference frame across the AM literature pertaining to evaluating texture in Ti-6Al-4V, which has resulted in the recommendation of a standard for the greater AM community based upon this work.

EBSD results show the same consistency of texture as a function of build height and the same deviations with scan strategy as compared to the neutron diffraction results. This is thought to stem from the texture memory effect previously documented in Ti-6Al-4V systems, where equivalent cooling rates produce the same α-Ti texture components, even after complete annealing in the β-Ti phase field [36.9, 36.12-13]. Even in the transformed microstructure, large as-solidified columnar grains were observed for the Raster scan strategy and finer, globular grains with colony $\alpha + \beta$ were observed for the Random and Dehoff scan strategies (**Figure 36.5**). The as-transformed microstructure of the Raster specimen demonstrated a fine, decomposed α' lath structure with fine dispersion of β-Ti. This suggests rapid cooling occurred during the build process and suppressed variant selection, thereby reducing the overall α-Ti texture observed. Subsequent layer depositions thermally decomposed the α' supersaturated with β-stabilizer(s) into the final build microstructures [36.14-16].

In order to initially evaluate the β-Ti texture for each specimen, a simulation of the $\beta \rightarrow \alpha$ transformation was completed using the MATLAB plug-in MTEX. This simulation used a {001} solidification fiber texture, given prior examples of β-Ti taking on this orientation [36.10, 36.12], and aimed to evaluate the solidification conditions of each scan strategy without necessitating EBSD reconstructions. The Random and Dehoff scan strategies showed remarkable agreement with the simulated α-Ti orientations, while the Raster scan strategy demonstrated less agreement with the simulated transformation orientations (**Figure 36.6**). This suggests the Raster scan strategy did not solidify with a {001} fiber texture, while the Dehoff and Random specimens did. EBSD reconstruction is required to confirm this.

A previously unreported α-Ti fiber texture, the $\{01\bar{1}2\}$, was identified amongst all three scan strategies and can be seen in the (0002) pole figures of **Figure 36.4**. This fiber texture constitutes the majority of the texture components for each specimen, and was found to be effectively parallel to the direction of suspected solidification, as informed by the simulation. This suggests a link between this fiber texture and the solidification direction, and is also thought to be an indication of certain solidification phenomenon. EBSD reconstruction was performed to evaluate this possibility, and to validate simulations.

36A.3 Recent Work

36A.3.1 β-Ti Reconstructions of EBM Ti-6Al-4V EBSD

Reconstruction of all large scale α-Ti EBSD maps was completed to evaluate the as-solidified grain size and texture (**Figure 36.7**). Evaluating 0-4 mm in build height, it was found that the Random and Dehoff scan strategies produce finer, freshly nucleated β-Ti grains (with Random having the finest as-solidified grain size). It was also found that the β-Ti demonstrated a {001} solidification fiber texture, as predicted by simulation, tilted towards the center of the aforementioned $\{01\bar{1}2\}$ fiber texture. This is indicative of non-eptiaxial solidification during the build process, as the β-Ti is free to orient around the {001} solidification direction, instead of inheriting the rotational position of previously solidified β-Ti [36.6-7]. The parallel orientation of the {001} fiber (direction of tilt is indicative of solidification direction) and the $\{01\bar{1}2\}$ fiber suggest α-Ti texture could be used as a direct evaluation of the as-solidified β-Ti and pre-transformation grain size. Finer grains would be indicative of fresh nucleation, which in turn can be identified by the presence of a {001} fiber texture. After transformation, this corresponds to a strong $\{01\bar{1}2\}$ fiber texture in the α-Ti, showing a simple assessment of α-Ti texture may be used to evaluate microstructural response in Ti-6Al-4V builds, without exhaustive destructive characterization.

The Raster reconstruction results enable a test of this theory. The as-solidified microstructure demonstrates large columnar grains, as initially shown by α-Ti EBSD mapping, and also demonstrates a cube texture in the (001) pole figure. This is indicative of epitaxial solidification, once again due to the constrained rotation of the solidifying β-Ti around the (001) axis, and the way in which orientations are propogated millimeters through the build height. Such a

microstructure must be considered with respect to the properties of as-built components, and again indicates how the presence of the $\{01\bar{1}2\}$ α fiber texture can be used to screen microstructures.

36A.4 Plans for Next Reporting Period

Future work will shift toward characterizing WAAM Ti-6Al-4V specimens, employing both large scale EBSD and bulk/local neutron diffraction experiments to see how microstructure and orientation change with build strategy. A neutron diffraction study on the texture memory effect of EBM Ti-6Al-4V specimens is also currently planned. Both facets of work are being prepared in a proposal for remote work to be completed at LANL on the HIPPO beam line. In parallel to this, a publication on the EBM Ti-6Al-4V texture results is in final preparation for submission to Acta Materialia. Future experiments will focus on evaluating the microstructural evolution of a Ti-Cu alloy to evaluate the genesis of grain refinement during AM processing.

- Submit proposal for texture memory effect and bulk/local texture measurements of EBM and WAAM Ti-6Al-4V with HIPPO to LANSCE at LANL.
- Complete large-scale EBSD of WAAM Ti-6Al-4V specimens and compare findings to previous EBM results.
- Summarize EBM Ti-6Al-4V microstructure and texture results and prepare/submit a peer-reviewed journal publication to Acta Materialia.
- Begin experiments to evaluate microstructure development of Ti-Cu alloy during simulated AM heating and cooling cycles.

36A.5 References

[36.1] B. Dutta, F.H. (Sam) Froes, The Additive Manufacturing (AM) of titanium alloys, Metal Powder Report. 72 (2017) 96–106.

[36.2] W. Frazier, Metal Additive Manufacturing: A Review, (2014).

[36.3] S. Liu, Y.C. Shin, Additive manufacturing of Ti6Al4V alloy: A review, Materials & Design. 164 (2019) 107552.

[36.4] W.J. Sames, F.A. List, S. Pannala, R.R. Dehoff, S.S. Babu, The metallurgy and processing science of metal additive manufacturing, International Materials Reviews. 61 (2016) 315–360.

[36.5] S.S. Al-Bermani, M.L. Blackmore, W. Zhang, I. Todd, The Origin of Microstructural Diversity, Texture, and Mechanical Properties in Electron Beam Melted Ti-6Al-4V, Metallurgical and Materials Transactions A. 41 (2010) 3422–3434.

[36.6] C.A. Brice, W.A. Tayon, A.L. Pilchak, Texture Development in Titanium Components Made by Additive Manufacturing, San Diego. (2014) 16.

[36.7] T.M. Butler, C.A. Brice, W.A. Tayon, S.L. Semiatin, A.L. Pilchak, Evolution of Texture from a Single Crystal Ti-6Al-4V Substrate During Electron Beam Directed Energy Deposition, Metallurgical and Materials Transactions A. 48 (2017) 4441–4446.

[36.8] P. Chandramohan, Laser additive manufactured Ti-6Al-4V alloy: Texture analysis, Materials Chemistry and Physics. 226 (2019) 272–278.

[36.9] I. Lonardelli, N. Gey, H.-R. Wenk, M. Humbert, S.C. Vogel, L. Lutterotti, In situ observation of texture evolution during α→β and β→α phase transformations in titanium alloys investigated by neutron diffraction, Acta Materialia. 55 (2007) 5718–5727.

[36.10] N.P. Gurao, S. Sethuraman, S. Suwas, Evolution of Texture and Microstructure in Commercially Pure Titanium with Change in Strain Path During Rolling, Metallurgical and Materials Transactions A. 44 (2013) 1497–1507.

[36.11] Y.N. Wang, J.C. Huang, Texture analysis in hexagonal materials, Materials Chemistry and Physics. 81 (2003) 11–26.

[36.12] S.C. Vogel, S. Takajo, M.A. Kumar, E.N. Caspi, A. Pesach, E. Tiferet, O. Yeheskel, Ambient and High-Temperature Bulk Characterization of Additively Manufactured Ti-6Al-4V Using Neutron Diffraction, JOM. 70 (2018) 1714–1722.

[36.13] G.C. Obasi, S. Birosca, J. Quinta da Fonseca, M. Preuss, Effect of β grain growth on variant selection and texture memory effect during α→β→α phase transformation in Ti–6 Al–4 V, Acta Materialia. 60 (2012) 1048–1058.

[36.14] H. Matsumoto, H. Yoneda, K. Sato, S. Kurosu, E. Maire, D. Fabregue, T.J. Konno, A. Chiba, Room-temperature ductility of Ti–6Al–4V alloy with α′ martensite microstructure, Materials Science and Engineering: A. 528 (2011) 1512–1520.

[36.15] W. Xu, M. Brandt, S. Sun, J. Elambasseril, Q. Liu, K. Latham, K. Xia, M. Qian, Additive manufacturing of strong and ductile Ti–6Al–4V by selective laser melting via in situ martensite decomposition, Acta Materialia. 85 (2015) 74–84.

[36.16] E. Sallica-Leva, R. Caram, A.L. Jardini, J.B. Fogagnolo, Ductility improvement due to martensite α′ decomposition in porous Ti–6Al–4V parts produced by selective laser melting for orthopedic implants, Journal of the Mechanical Behavior of Biomedical Materials. 54 (2016) 149–158.

36A.6 Figures and Tables

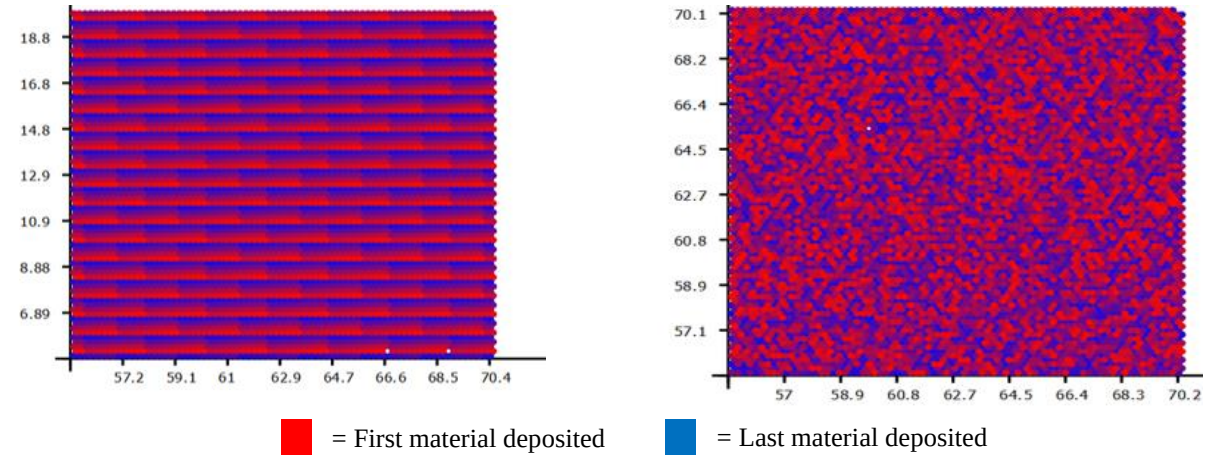

Figure 36.1: Illustrations of the two spot melt scan strategies Dehoff (left) and Random (right).

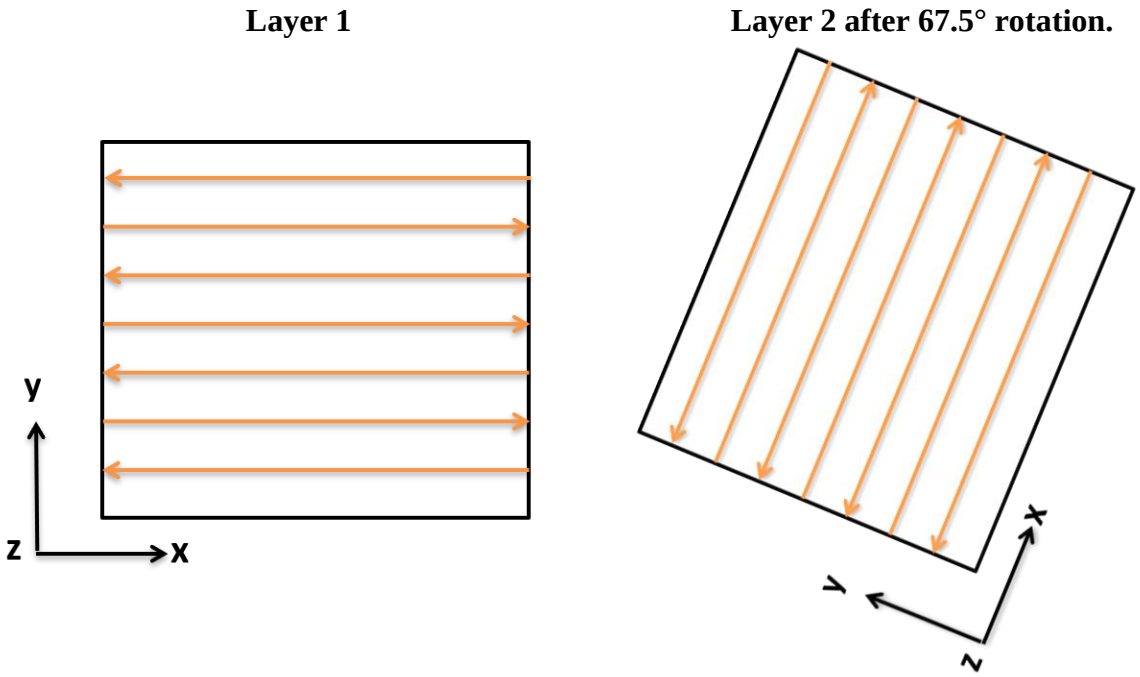

Figure 36.2: Illustration of the Raster scan strategy. Note the 67.5° rotation between layers incorporated into this build process (right).

Figure 36.3: WAAM Ti-6Al-4V samples extracted for characterization (courtesy of SNL).

Scan Strategy	Bulk	1 mm Build Height	13 mm Build Height	23 mm Build Height
Dehoff α-Ti	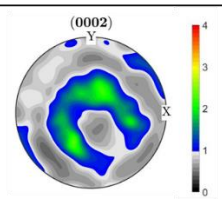	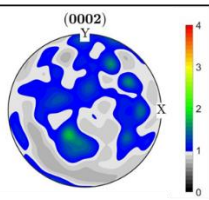	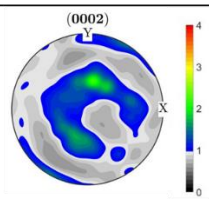	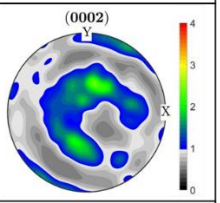
Random α-Ti	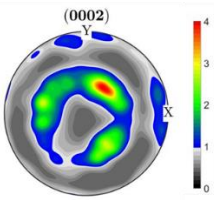	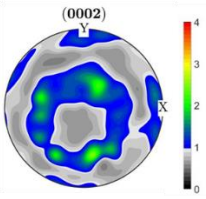	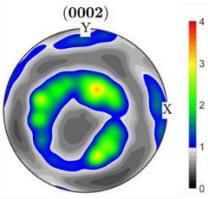	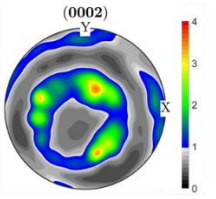
Raster α-Ti	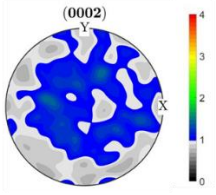	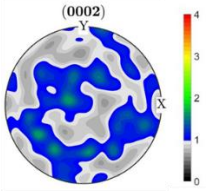	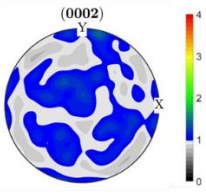	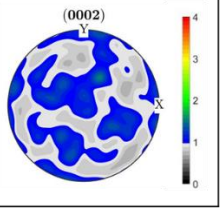

Figure 36.4: α-Ti neutron diffraction pole figures demonstrating consistent texture as a function of build height, but variations between scan strategies. Note the build direction is oriented out of the page and the clear presence of the $\{01\bar{1}2\}$ fiber texture in all (0002) pole figures.

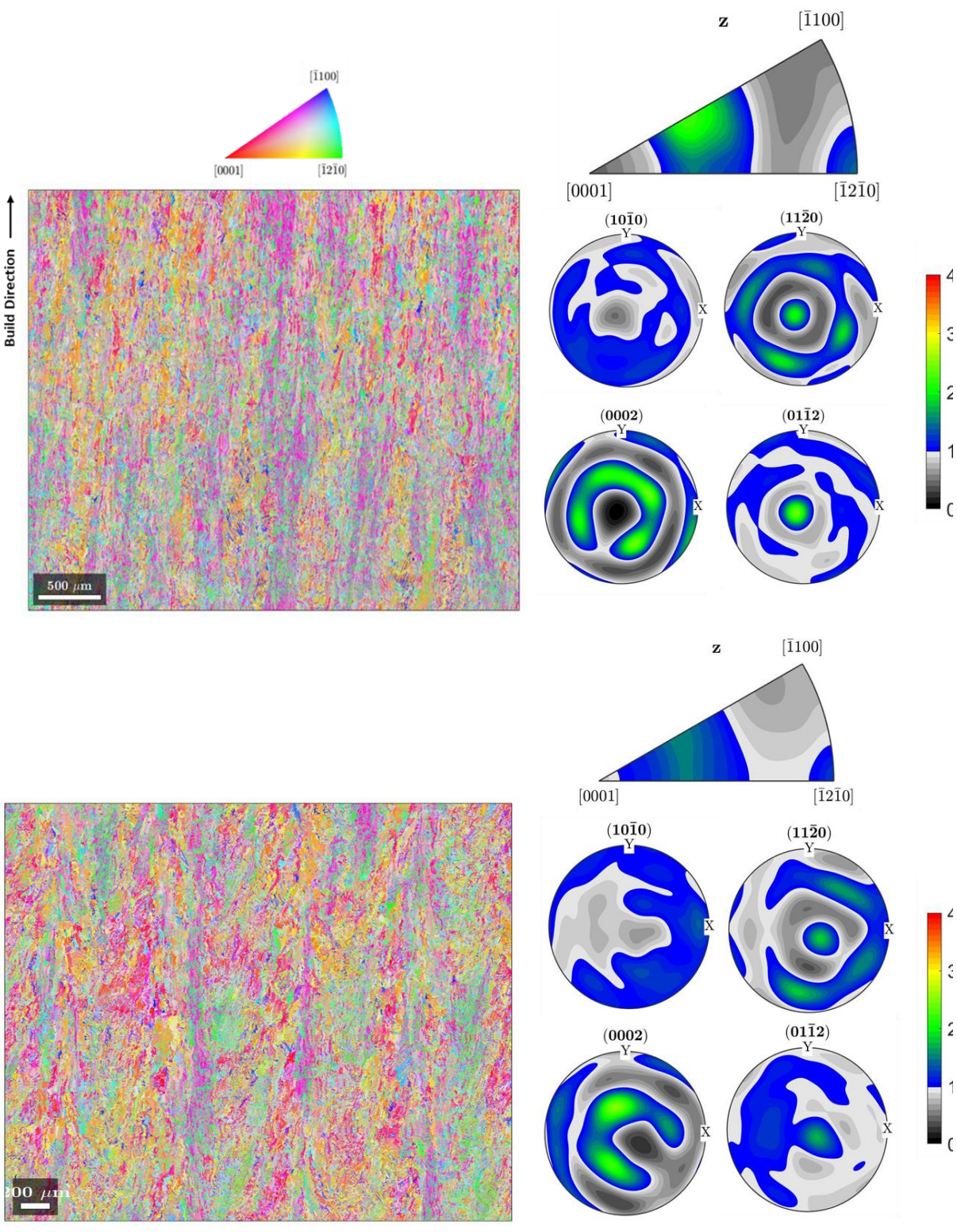

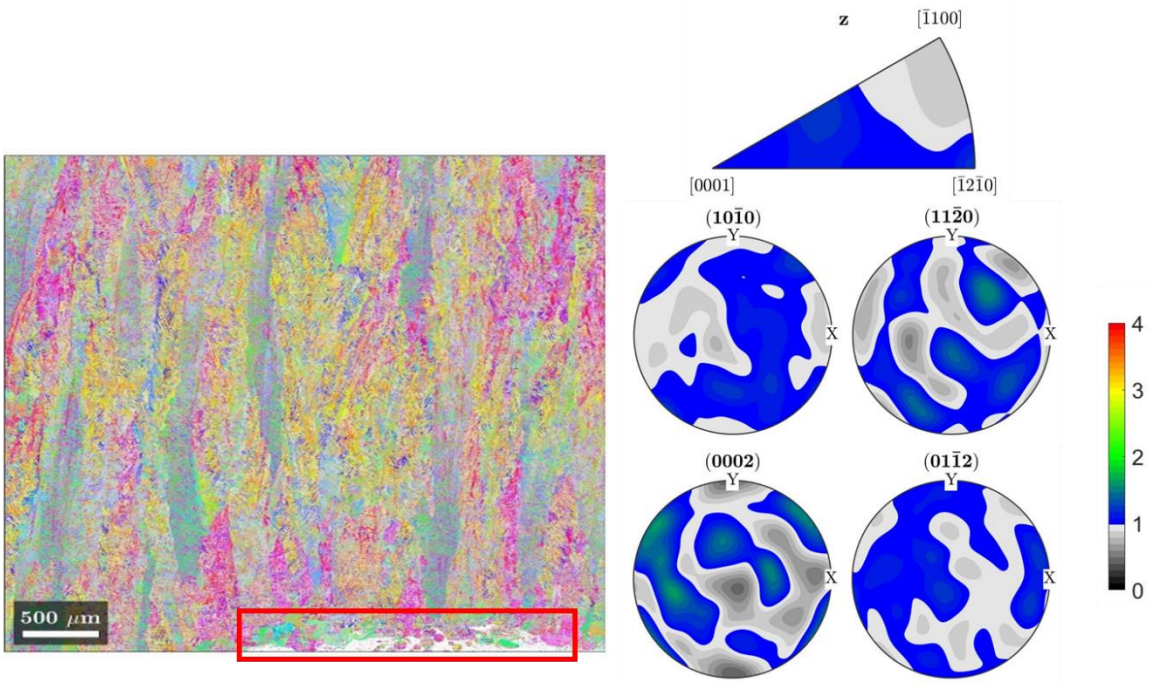

Figure 36.5: α-Ti EBSD inverse pole figure (IPF) maps, pole figures, and inverse pole figures of the Random (top), Dehoff (middle), and Raster (bottom) scan strategies from 0-4 mm in build height. Note the clear presence of large-columnar grains in the Raster scan strategy, which are not present in the two spot melt scan strategies. The red rectangular section of the Raster IPF map is a region of left-over β-Ti from the build process, due to Fe- and Cr-enrichment from the base plate.

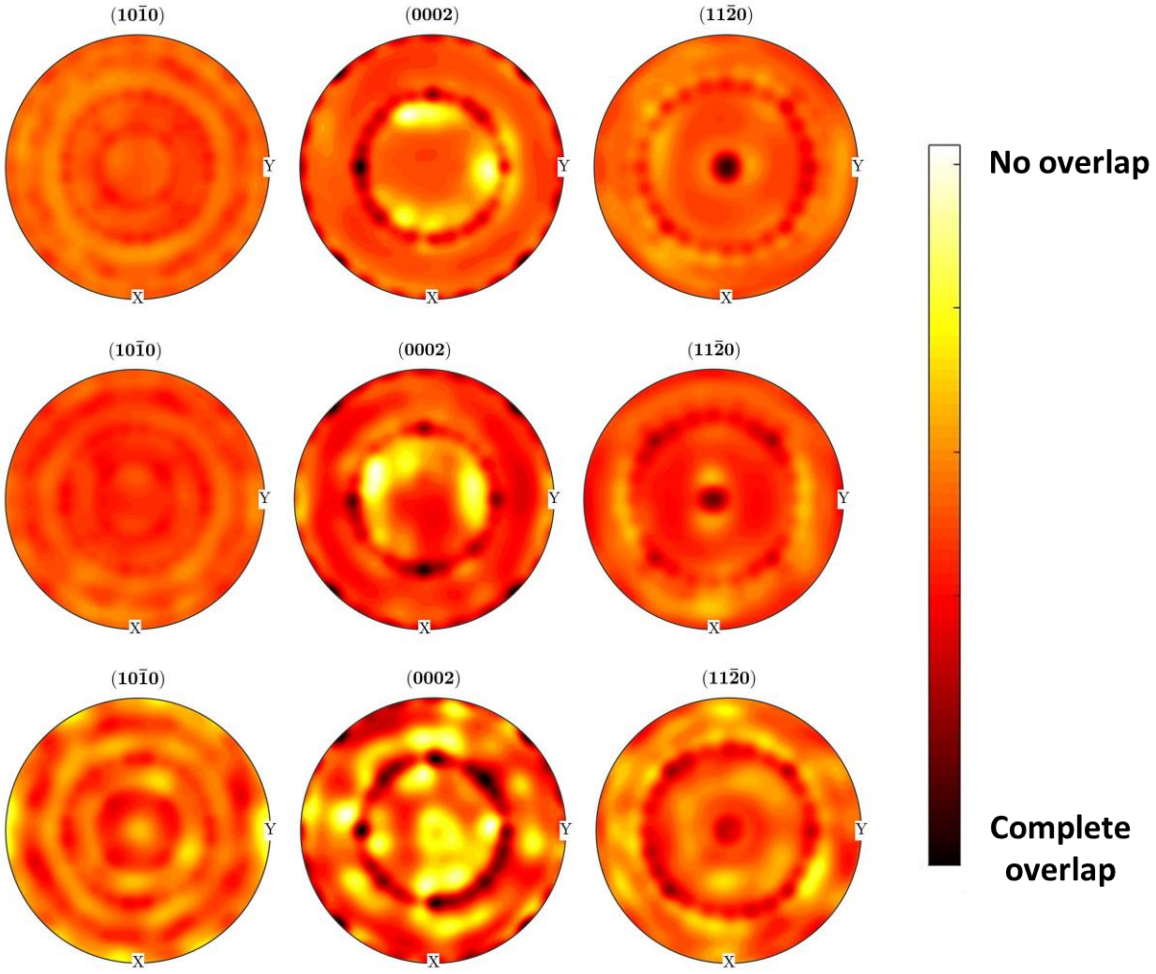

Figure 36.6: Heat maps illustrating the overlap of simulated and neutron diffraction measured α-Ti orientations for the Random (top), Dehoff (middle), and Raster (bottom) EBM Ti-6Al-4V scan strategies. Note the Random and Dehoff plots demonstrate remarkable agreement, while the Raster scan strategy demonstrates little to no overlap. This indicates a {001} solidification fiber texture was not applicable for the Raster scan strategy, but is observed for the Random and Dehoff scan strategies.

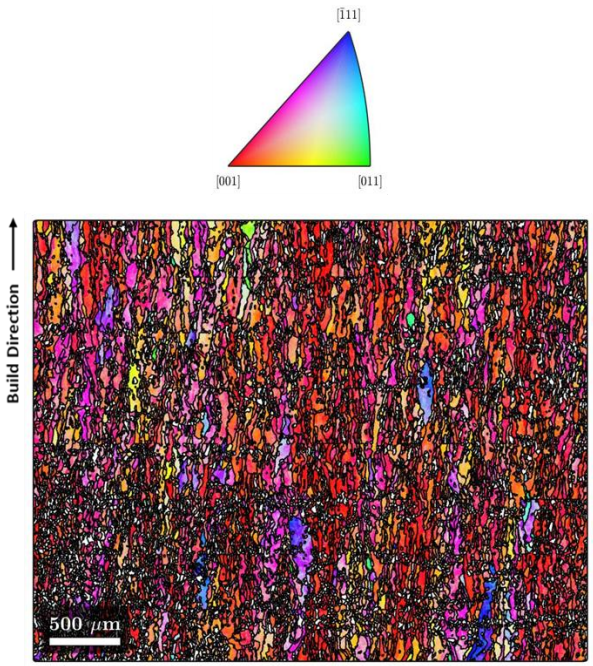

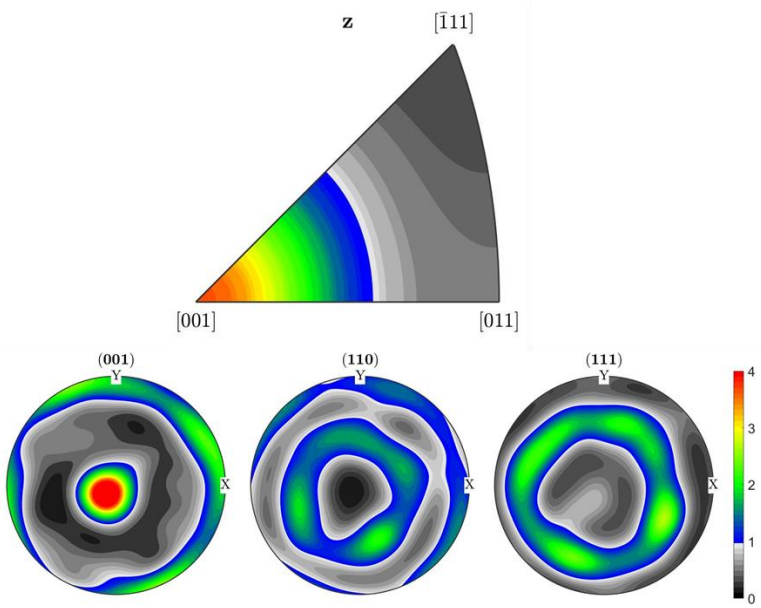

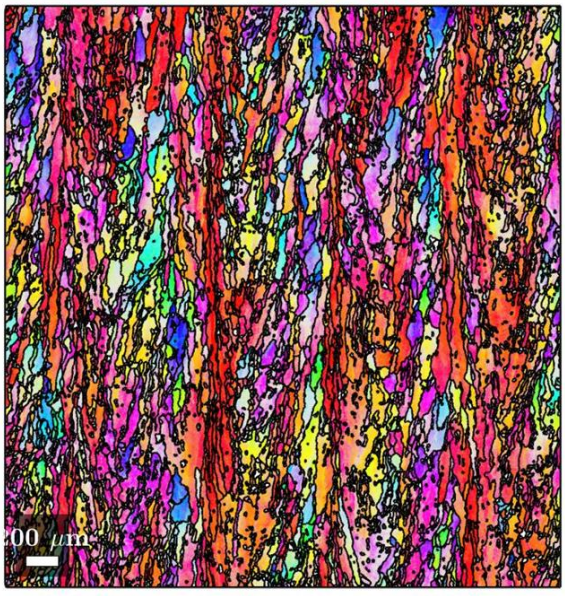

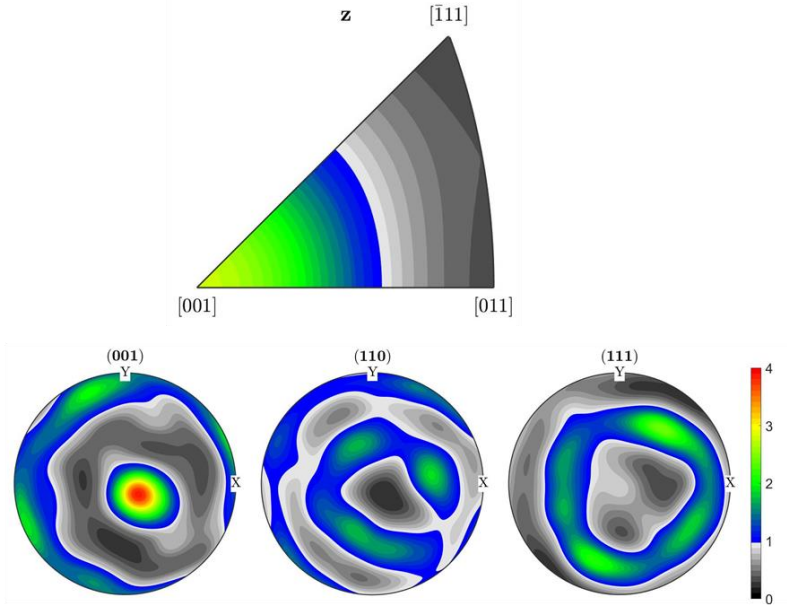

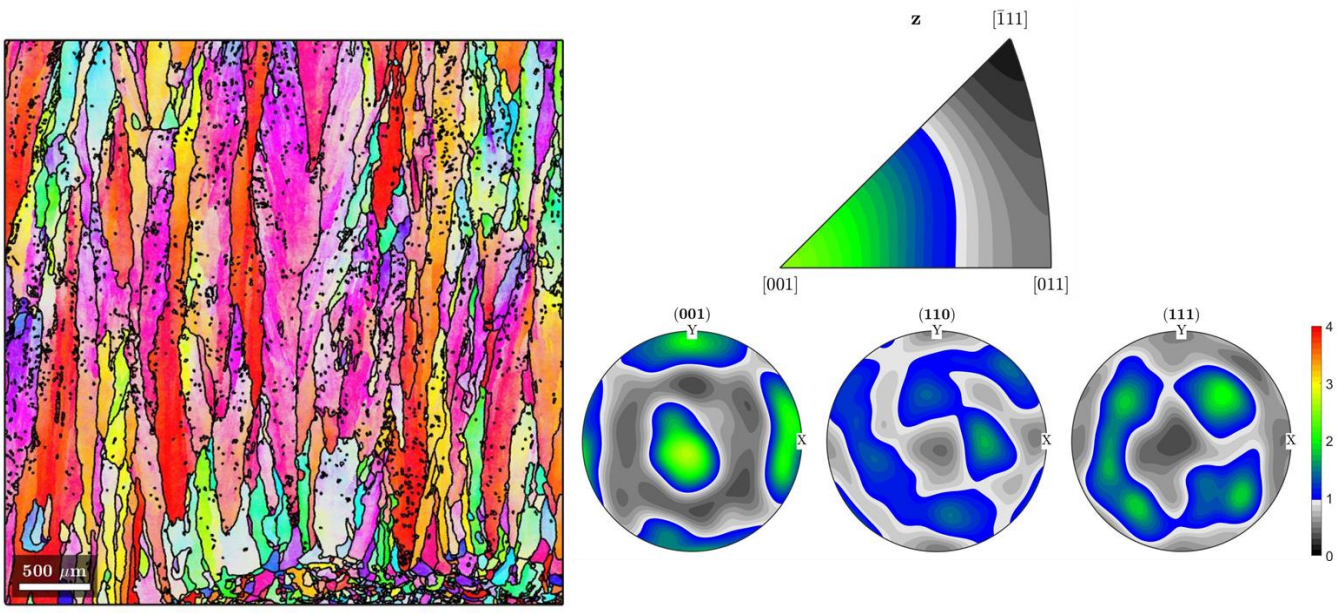

Figure 36.7: Reconstructed β-Ti IPF maps, pole figures, and inverse pole figures for the Random (top), Dehoff (middle), and Raster (bottom) scan strategies. Note the clear difference in as-solidified grain sizes between the spot and Raster scan melt strategies, along with a change from a {001} fiber texture to a cube texture for the spot and raster melt scan strategies, respectively.